Research article

Lu Huang, Yaqiang Qin, Yunfeng Jin, Hao Shi, Honglian Guo, Liantuan Xiao* and Yuqiang Jiang*

Spheroidal trap shell beyond diffraction limit induced by nonlinear effects in femtosecond laser trapping

https://doi.org/10.1515/nanoph-2020-0288
Received May 15, 2020; accepted July 30, 2020; published online August 21, 2020

Abstract: Beyond diffraction limit, multitrapping of nanoparticles is important in numerous scientific fields, including biophysics, materials science and quantum optics. Here, we demonstrate the 3-dimensional (3D) shell-like structure of optical trapping well induced by nonlinear optical effects in the femtosecond Gaussian beam trapping for the first time. Under the joint action of gradient force, scattering force and nonlinear trapping force, the gold nanoparticles can be stably trapped in some special positions, or hop between the trap positions along a route within the 3D shell. The separation between the trap positions can be adjusted by laser power and numerical aperture (NA) of the trapping objective lens. With a high NA lens, we achieved dual traps with less than 100 nm separation without utilizing complicated optical systems or any on-chip nanostructures. These curious findings will greatly extend and deepen our understanding of optical trapping based on nonlinear interaction and generate novel applications in various fields, such as microfabrication/nanofabrication, sensing and novel micromanipulations.

Keywords: diffraction limit; nonlinear effects; optical trapping.

1 Introduction

Optical tweezers have become a versatile tool that is widely applied in various research areas, especially in biophysical studies, materials science and soft condensed matter physics [1–6]. In the conventional optical tweezers, a continuous wave (CW) laser is usually used for light source, and the trapping is realized based on the linear interaction between sample and light. A Gaussian beam focused by a high NA lens generates only one trap, while the multitraps in 3-dimension (3D) can be obtained by the approaches of beam splitting [7–9], time sharing [10–12] or diffractive optics [13–21]. For conventional optical tweezers based on the far-field technique with lens or microscope objectives, its performance is inevitably limited by diffraction, and the distance between traps cannot be smaller than the diffraction limit. Although some strategies relying on strong near-field concentration of plasmonic nanostructures are carried out [22–24], these manipulations are usually confined in the region near surface, which greatly limits their applications.

Reducing the size of the trapped particle results in a sharp decrease in the gradient force and a shallower trapping potential well; hence, it is a challenge to trap nanoparticles with conventional optical tweezers. The use of ultrashort laser pulses instead of CW lasers as trapping source in optical tweezers give some advantages when the target particles are in the Rayleigh regime. In comparison to conventional CW optical tweezers, the distinctive feature

Lu Huang, Yaqiang Qin and Yunfeng Jin have same contribution to the work.

***Corresponding authors: Liantuan Xiao**, Collaborative Innovation Center of Extreme Optics, Shanxi University, Taiyuan, Shanxi, 030006, China, E-mail: xlt@sxu.edu.cn; **Yuqiang Jiang**, State Key Laboratory of Molecular Developmental Biology, Institute of Genetics and Developmental Biology, Innovation Academy for Seed Design, Chinese Academy of Sciences, Beijing, 100101, China; University of Chinese Academy of Sciences, Beijing, 100049, China; and Collaborative Innovation Center of Extreme Optics, Shanxi University, Taiyuan, Shanxi, 030006, China, E-mail: yqjiang@genetics.ac.cn
Lu Huang and Yaqiang Qin, State Key Laboratory of Molecular Developmental Biology, Institute of Genetics and Developmental Biology, Innovation Academy for Seed Design, Chinese Academy of Sciences, Beijing, 100101, China; University of Chinese Academy of Sciences, Beijing, 100049, China. https://orcid.org/0000-0002-1754-9708 (L. Huang). https://orcid.org/0000-0002-5633-7417 (Y. Qin)
Yunfeng Jin and Hao Shi, State Key Laboratory of Molecular Developmental Biology, Institute of Genetics and Developmental Biology, Innovation Academy for Seed Design, Chinese Academy of Sciences, Beijing, 100101, China
Honglian Guo, Minzu University of China, Beijing, 100081, China

of trapping with ultrashort laser pulses is the nonlinear optical effects in the trapped particles induced by the high impulsive peak powers [25–32]. Femtosecond (fs) lasers can be used for optical trapping and simultaneously utilized to induce nonlinear two-photon processes. A more fascinating trapping behavior induced by the nonlinear optical effects is called "trap split", in which the trapping potential well of the gold nanoparticle (GNP) splits into two off-axis subwell along the polarization direction of femtosecond trapping laser [32].

In this paper, we report novel optical manipulations based on the nonlinear optical effects. An ellipsoidal shell-like 3D potential well formed by the effects of trap split is experimentally demonstrated for the first time. By applying an orthogonal illuminating and imaging system, the motion of the trapped GNPs along the shell-like potential well is observed. Some characteristic points on the shell, where the GNPs can be stably trapped form multiple traps. Compared to the previous methods that formed multitraps, such as time sharing or diffractive optics, this nonlinear-based method have much simpler optical design and optical system. The most attractive feature of nonlinear optical trapping is the separation of the subtraps breaks the diffraction limit. Unlike near-field plasmonic tweezers which need complex nanofabrication to form the beyond diffraction-limit particle manipulation, we realized multiple GNPs trapping beyond the diffraction-limit in far-field with a microscope objective and a femtosecond Gaussian laser beam. These works will greatly deepen and extend our understanding about the optical trapping based on nonlinear effects, and generate wide applications in the fields of optical manipulations, microfabrications, optical printing, and so on.

2 Theoretical analysis and numerical simulations

In the Rayleigh region, the nanoparticles in electrical field can be treated as dipoles. When the nanoparticles are trapped by a CW laser, the interaction between the particles and the electric field of light is linear, so the polarization can be expressed as $\mathbf{P} = \varepsilon_0 \chi \mathbf{E}$, where ε_0 is permittivity of free space, χ the electric susceptibility of the particles, and $\mathbf{E}$ the electric field of light. In the case of fs laser trapping of nonlinear nanoparticles, however, the nonlinear effects will become prominent, so the electric polarization of the particles can be given by $\mathbf{P} = \varepsilon_0 (\chi_1 + \chi_3 |\mathrm{E}|^2)\mathbf{E} = \varepsilon_0 (\chi_1 + \chi_3 I)\mathbf{E}$, where χ_1 and χ_3 are the linear and nonlinear electric susceptibility of the particles, and I is the intensity of electric field. If the fs laser is assumed to be a Gaussian beam with the transverse electromagnetic (0,0) (TEM_{00}) mode, then at the focal plane, $I = I_0 \exp(-2\rho^2)$, where ρ is the radial distance from beam center. The interaction potential is given by the following equation when the scattering force is negligible,

$$\begin{aligned}\langle U_P \rangle &= -\langle \mathbf{P} \cdot \mathbf{E} \rangle \sim -\varepsilon_0 \chi_1 (I - aI^2) \\ &= -\varepsilon_0 \chi_1 I_0 \cdot \exp(-2\rho^2)[1 - aI_0 \cdot \exp(-2\rho^2)]. \end{aligned} \quad (1)$$

$\langle U_P \rangle$ denotes the time averaged potential over the optical cycle. $a = -(3/4)(\chi_3/\chi_1)$ is a function of laser frequency and aI_0 reflects the degree of nonlinear polarization. The condition for the extremal values of $\langle U_P \rangle$ is found to be $\rho \exp(-2\rho^2) = 0$ or $1 - 2aI_0 \exp(-2\rho^2) = 0$. As aI_0 increases from zero, the potential minimum is found initially located at the beam center ($\rho = 0$), and then splits when $aI_0 > 1/2$. The minima of $\langle U_P \rangle$ appear at the positions of $\rho_0 = [\ln(2aI_0)/2]^{1/2}$, i.e., the trap position under fs laser splits from focal point into a circle with radius of ρ_0.

The split of potential well suggests a distinct interaction from conventional optical tweezers. The trapping force exerted on the GNP can be expressed as following after considering the nonlinear polarization,

$$\begin{aligned}F_G \sim -\nabla U_P(\rho) &= -4\rho\varepsilon_0\chi_1 I_0 \cdot \exp(-2\rho^2) \\ &\quad + 8a\rho\varepsilon_0\chi_1 I_0^2 \cdot \exp(-4\rho^2). \end{aligned} \quad (2)$$

The first term in Eq. (2) arises from linear interaction between light and GNPs, which is corresponding to the gradient force in conventional optical trapping, we name it as "linear optical trapping force", $F_L = -4\rho\varepsilon_0\chi_1 I_0 \cdot \exp(-2\rho^2)$; while the second term indicates a new kind of interaction, which is derived from nonlinear polarization caused by fs laser, we name it as "nonlinear optical trapping force", i.e., $F_{NL} = 8a\rho\varepsilon_0\chi_1 I_0^2 \cdot \exp(-4\rho^2)$. The linear, nonlinear and the resultant forces are calculated with various values of aI_0, as shown respectively in Figure 1(a)–(c). It is worth noting that the directions of the two kinds of trapping forces, linear and nonlinear, are opposite. The linear trapping force confines the particles in beam axis (point O) while the nonlinear trapping force pushes them away from beam axis. When aI_0 is less than 1/2, the amplitude of linear optical trapping force is larger than that of the nonlinear one, so the particles will be confined in the beam center, similar to that of the conventional CW trapping. When aI_0 is larger than 1/2, however, the nonlinear effects are dominant as the amplitude of nonlinear optical trapping force is larger. Therefore, the resultant force pushes the particles away from beam axis and reaches equilibrium

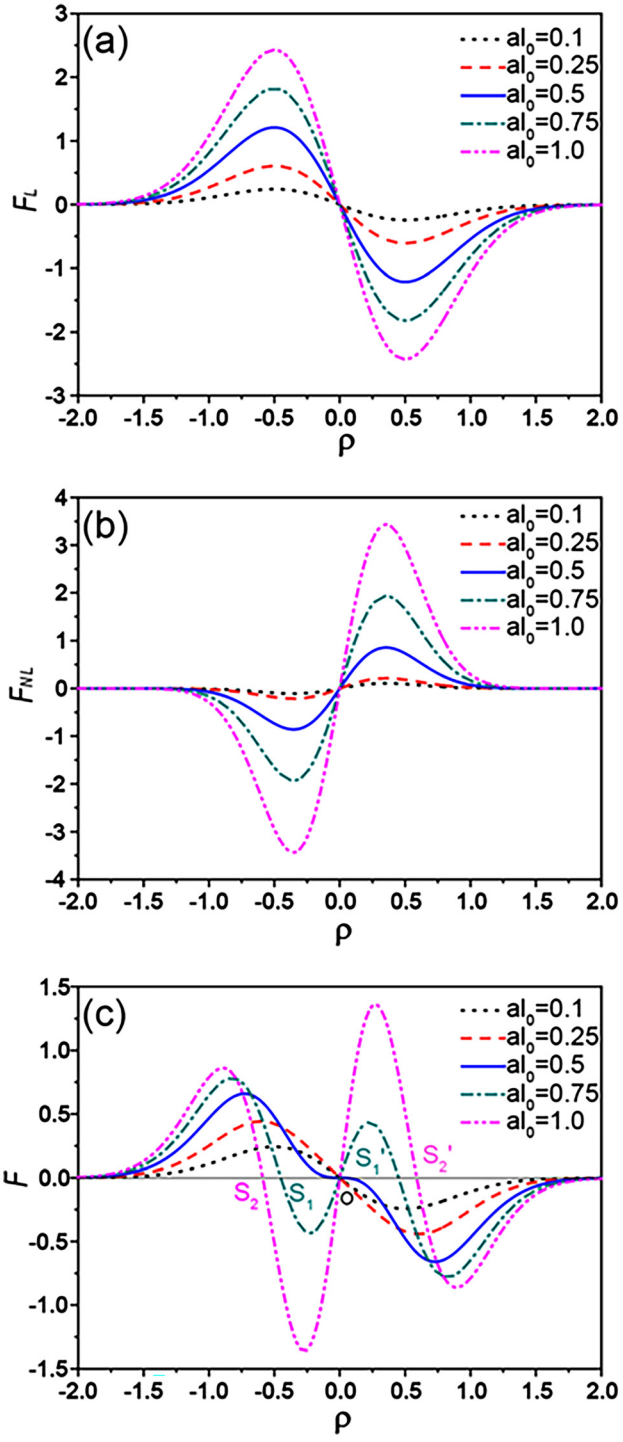

Figure 1: The optical trapping forces in the femtosecond (fs) laser trapping of gold nanoparticle (GNPs).
(a)–(c) The linear component, nonlinear component and resultant force, respectively.

at the position of $\rho_0 = [\ln(2aI_0)/2]^{1/2}$, as shown by points S_1, S_1', S_2 and S_2' in Figure 1(c). i.e., the trap position splits into a circle with radius of in focal plane.

In the case of the laser intensity is very strong, higher order nonlinear polarization should also be considered. After expanding the nonlinear polarization up to fifth order (for details, see Supplementary material), the experimental results could be fitted very well according to the theoretical analysis, as shown in Figure S2. We also found the main features of nonlinear trapping force considering fifth order polarization is very similar to that of expanded up to third order, as shown in Figure S3.

It is worth noting that we analyse the nonlinear effect based on the perturbation expansion of the polarization in the paper [32–34]. The theoretical analysis qualitatively illustrates the basic concept and main characteristics in this novel nonlinear trapping. For rigorous analysis, a calculation with nonperturbative method used in the papers published by Kudo [35] and Hoshina [36] could be referred.

If we neglect the polarization of light, the potential energy along the split circle should be identical. That means the trapped particles may locate in any position on the circle. In the case of tightly focusing of linear polarized laser beam, however, the trapping potential energy in the direction of polarization will be lower, as shown in the following analysis.

The trap split is not limited in the focal plane but occurs in all the 3D focal volume. When the linearly polarized light beam is tightly focused, the electrical field distribution of light beam in the focal region can be calculated by the vector diffraction theory [37–39],

$$\mathbf{E}(\rho,\varphi,z) = \frac{\mathrm{i}kf e^{-\mathrm{i}kf}}{2\pi}\int_0^{\theta_{\max}}\int_0^{2\pi}\mathbf{E}_\infty(\theta,\phi)e^{\mathrm{i}kz\cos\theta}e^{\mathrm{i}k\rho\sin\theta\cos(\phi-\varphi)} \times \sin\theta\ \mathrm{d}\phi\ \mathrm{d}\theta. \tag{3}$$

Then the potential energy of trapped GNPs in all the focal volume can be calculated by combining Eqs. (1) and (3). Figure 2 shows the calculated results of the potential energy in the focal volume when the GNPs are trapped by linearly polarized fs laser beam in Gaussian mode. Here set $aI_0 = 1$, the wavelength of fs laser is set to be 840 nm, and the filling factor (the ratio of the beam diameter to the back aperture size of the objective lens) is set to be 9.5/8 in the theoretical simulation. We define the direction of light polarization as X axis, and the direction of light propagation as Z axis. The strong focusing of linearly polarized Gaussian beam, especially the generation of longitudinal component of light field, makes the distribution of potential energy no longer circular uniform. Figure 2(a) shows the distribution of trapping potential in transverse (XOY) planes with different z values, it is very interesting that all

the radial minima in the focal volume constitute an ellipsoidal shell, we name it as "trap split shell (TSS)". The distribution of potential energy in XOY, XOZ and YOZ is shown in Figure 2(b)–(d), respectively. The potential minima in XOY, XOZ and YOZ are indicated by the curves L_1, L_2 and L_3, respectively, and the values are compared in Figure 2(e). It is very clear that the potential values at points A and B are the lowest within the TSS. The potential difference between points A (or B) and C (or D), i.e., the height of potential barriers between A and B within TSS, is dependent on the trapping laser power. When laser power is high enough, the trapped particles will be confined at points A and (or) B, and this should be corresponding to the reported "trap split" [32].

Although the light field is still in Gaussian mode, the nonlinear effect of GNPs in fs pulses generates a shell-like potential energy well. And a very important feature of the split shell is its small size. Figure 2(f) shows the profiles of light intensity and trapping potential energy in the focal plane. The shell-like potential well generated by nonlinear effects, including points A and B, are confined within the beam profile, and the transversal diameter changes with the light intensity, $\rho_0 = [\ln(2aI_0)/2]^{1/2}$. For a focused Gaussian beam, the intensity profile can be adjusted by the numerical aperture (NA) of objective lens, so the sophisticated trapping structure beyond diffraction limit could be achieved.

3 Experimental results

To observe the 3D structure of shell-like potential well, we built an orthogonal illuminating and imaging system. The schematic diagram of experimental setup is shown in Figure S1 in Supplementary material. Preliminarily we used a relatively low NA objective lens (NA = 0.65) for optical trapping and front-view imaging. The linearly polarized Ti: sapphire laser was first set to be CW mode, and only one trap position was observed when the GNPs were trapped. When the laser was switched to fs pulsed mode, the trapping position split from one point into two points along the polarization direction.

The trap split was highly dependent on the power of the trapping laser. When the laser power was higher than 450 mW, the particles were stably trapped. However, when the power of the laser decreased, the trapping became unstable, and the particles might jump between the two split trap positions. We define a coordinate system in which the CW trapping point is set as origin, the direction of polarization as *X* axis and the propagating direction of light as *Z* axis. When we observed the particles in XOY plane, they usually jumped directly between the two positions, as indicated by the green arrows in Figure 3(a) (see Supplementary video 1, front-view). These processes were also observed by the other imaging system (side objective lens [SOLs] and cam 2 in Figure S1). We found that the trapping of GNPs gradually became unstable in longitudinal direction with the decrease of the laser power. The Brownian motion of particles became more and more obvious, until the particles escaped from one trap and moved to the other one. As expectation, this motion is along an oval trajectory in longitudinal direction (within XOZ plane), as indicated by the green line in Figure 3(b) (see Supplementary Video 1, side-view). We also noticed that the oval motion trajectory was always along downstream of laser light propagation. With the power of fs laser further decreasing, the jumping became more and more frequent, meanwhile another type of motion which is along a circular trajectory in XOY plane was also observed, as shown in Figure 3(c) (see Supplementary Video 2, front-view). In side-view, the particles were observed hopping from one position to the other, as shown in Figure 3(d) (see Supplementary Video 2, side-view). The probabilities of these two types of motion were dependent on laser power. At relative high power, the jumping is mainly in XOZ plane. With the decrease of power, the probability of motion in XOZ plane decreased while that in XOY plane increased, as shown in Figure 4(a).

The distance between trapping points (A and B in Figure 3) is dependent on the trapping laser power. With decreasing the power of fs laser, the distance became small and small, as shown in Figure 4(b). By Gaussian fitting at the trapped particle intensity (Figure S4), the trap position and separation distance can be easily measured. While the trap separation is beyond the diffraction limit, we determined each trap position, respectively, using the method of single molecule localization technique by adjusting the concentration of the GNPs to ensure only one particle was trapped. Another two objective lenses of NA = 0.95 and NA = 1.40 were also employed for optical trapping instead of the one of NA = 0.65. The separation distance gets smaller as the laser power decreasing, and broke the diffraction limit for all the three objectives of different NA, as shown in Figure 4(b).

4 Discussions

The experimental results (Figure 3(a)–(d)) clearly demonstrated the 3D structure of spherical shell-like potential well generated by the nonlinear effects, i.e., the TSS described in Figure 2(a). Although the trapping well is

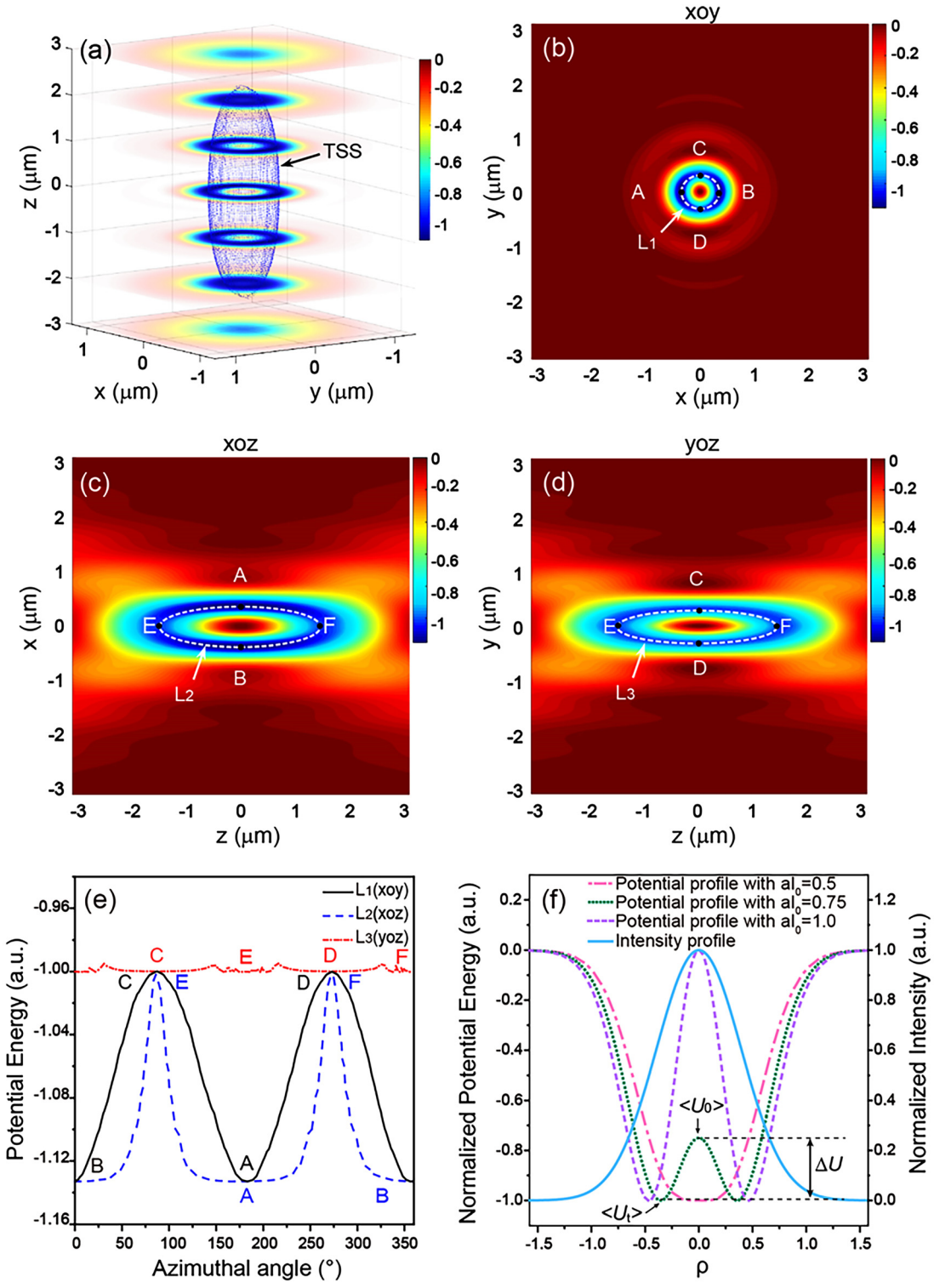

Figure 2: Numerical simulated potential energy of the trapped gold nanoparticle (GNP) in a femtosecond (fs) laser Gaussian beam. The propagation direction of the trapping beam is along *z* axis, and the direction of polarization is along *x* axis.
(a) The three-dimensional (3D) distribution of potential energy of trapped GNPs in the focal volume; (b)–(d) potential energy of trapped GNPs in XOY, XOZ and YOZ planes, respectively. The white dashed lines indicate the minima of potential energy; (e) comparison of potential minima in the three planes (L_1 in XOY, L_2 in XOZ and L_3 in YOZ); (f) the profiles of light intensity and trapping potential energy in the focal plane. The potential with different al_0 also showed. In all figures, the potential energy is normalized to the value of point C or D.

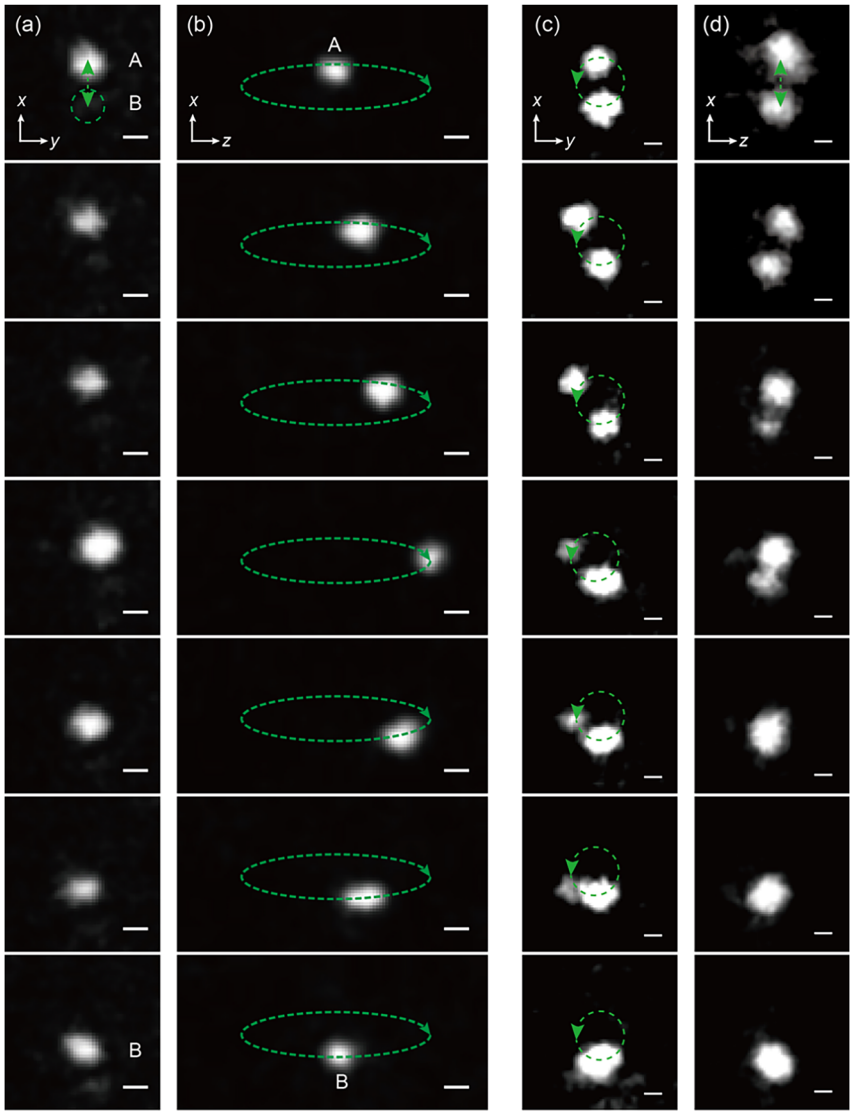

Figure 3: Experimental results of femtosecond (fs) trapping. Column (a) gold nanoparticles (GNPs) trapped by fs laser, the green arrows indicate the jumping motion in XOZ plane of GNP between the two split positions viewed by the front objective lens (FOL in Figure S1); (b) the motion of GNP(s) shown in (a) viewed by the side objective lens (SOLs in Figure S1), the green curve and arrows show the trajectory of particles motion; (c) the circular motion in XOY plane of GNPs between the two trap positions viewed by FOL when laser power is relative low; the green curves indicate the trajectory of particles motion; (d) the motion of GNP(s) shown in (c) viewed by the SOLs, the green curve and arrows show the trajectory of particles motion. In all figures, the polarization is along *x* direction, and the light propagates along *Z* axis. Scale bar: 1 μm.

shell-like, and the potential energy at each point on the shell is radial minimum, the strong focusing of linear polarized light beam makes the potential on the shell not identical anymore because the obvious *z* component of electric field is generated. The potential energy at points A and B becomes lower than the others. When laser power is high enough (e.g., 450 mW in our experiments), the potential difference between points A (or B) and C (or D), i.e., the height of potential barriers between A and B within the TSS is large enough (more than a few k_BT), so the trapped particles will be confined at points A and (or) B. When the laser power decreases, the potential barriers between points A and B become lower and lower, so the particles trapped at points A or B may jump from one position to the other one because of Brownian motion or other disturbance. Meanwhile, the potential energy on the TSS is radial minimum, then the motion of trapped particles must be confined within the TSS.

There are two potential barriers between point A and B both in L_1 and in L_2 (shown in Figure 2(e)). As the potential barrier between points A and B in XOY plane is similar to that in XOZ, there are two possible routes for the GNPs hopping (L_1 or L_2) within the TSS, and this has been demonstrated in our experiments, as shown in Figure 3. From Figure 2(e), the potential energy near points A and B along L_2 is much flatter than that along L_1, so it is easy to understand that the stability of particles in longitudinal (*Z*) direction is less than that in lateral directions. However, the simulation results in Figure 2 cannot explain the different hopping probability along L_1 and L_2, and why the jumping always locates in the downstream of trapping points (A and B).

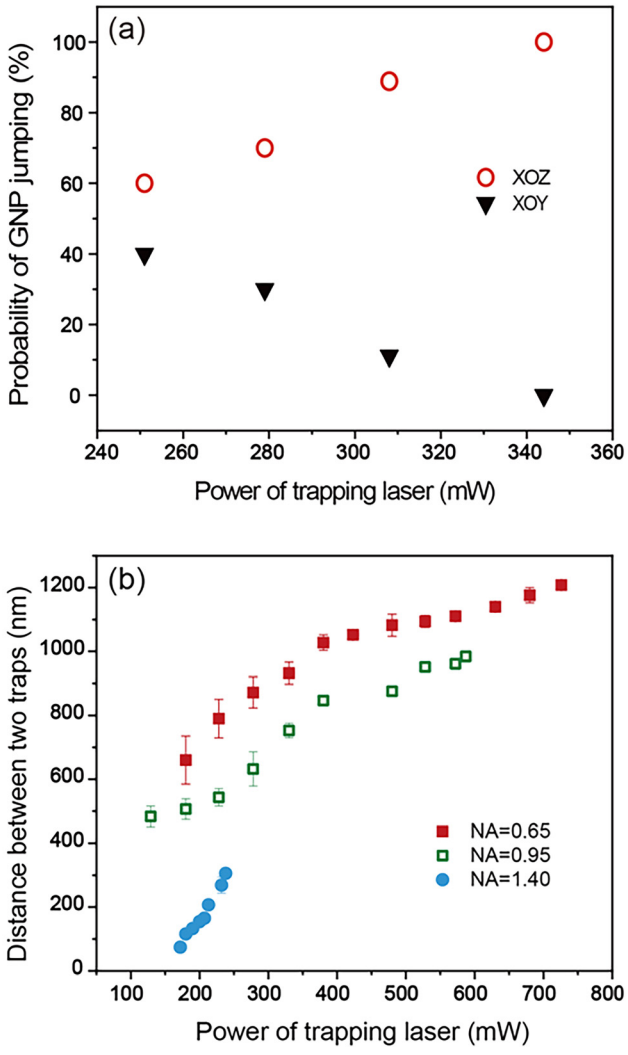

Figure 4: Beyond diffraction limit multiparticle manipulation with femtosecond (fs) Gaussian beam laser.
(a) The probability of gold nanoparticles (GNPs) hopping in the XOZ and XOY planes measured in the experiments; (b) The trap separations beyond the diffraction limit as the trapping power decreased. Data of trapping objectives with different NA also showed.

For a particle trapped in a tightly focused laser pulse, the transverse scattering force is several orders of magnitude smaller than the gradient force [33], the scattering force as shown in Figure S5 in the Supplementary material. The longitudinal scattering force will become significant or even dominant in the case of GNPs trapping because of the strong scattering and absorption of light by the particles, but it does not account for the generation of trap split, as while as the 3D structure of potential well because the scattering is axisymmetric and monotonically along the light propagation. To avoid the complexity and clearly demonstrate the significant and the domination role of the nonlinear effect in the 3D shell-like potential well formation, the scattering force was neglected in all above analysis. Although scattering force has little influence on the structure of shell-like potential well, it greatly affects the trapping behaviors, especially in the longitudinal plane, as shown in the following.

The scattering force can be expressed as

$$F_{sc} = n_m \cdot \langle S \rangle C_{sc}/c. \tag{4}$$

where n_m is the refractive index of surrounding, C_{sc} the scattering cross section of GNP, c the speed of light, and <S> the Poynting vector, which can be expressed as

$$\begin{aligned}\langle S \rangle &= \frac{1}{2}\mathrm{Re}\left[\vec{E} \times \vec{H}^*\right] \\ &= \frac{1}{2}\mathrm{Re}\left[\left(E_y H_z^* - E_z H_y^*\right)\vec{i} + \left(E_z H_x^* - E_x H_z^*\right)\vec{j} \right. \\ &\quad \left. + \left(E_x H_y^* - E_y H_x^*\right)\vec{k}\right].\end{aligned} \tag{5}$$

The distributions of lateral and longitudinal components of scattering force in XOY and XOZ planes are calculated, as shown in Figure S5. The amplitude of lateral component is two orders less than the longitudinal one. The scattering force generates additional potential difference in the focal region and greatly affects the behaviors of the trapped GNPs in fs laser trapping. The distribution of potential energy in XOZ plane after considering scattering force is calculated, as shown in Figure 5(a). The potential distributions along L_2 under various trapping power are shown in Figure 5(b). The potential value at point F decreases because of the scattering effect while that at point E increases, so the upstream potential barrier, $U_{A'EB'}$, is higher than the downstream one ($U_{A'FB'}$) after considering the scattering force. That is why the GNPs always move along downstream route when they hop between trapping positions, as we observe in the experiments. The positions of minima (i.e., trapping positions) also shift from points A and B to points A′ and B′ because of scattering force (Figure 5(a, b)). The distributions of potential minima in lateral plane where the points A′ and B′ are included after considering scattering is also calculated, as shown in Figure 5(c). The potentials along L_1' in Figure 5(c) under different trapping intensity are shown in Figure 5(d). The value of potential barriers between points A′ and B′ ($U_{A'C'B'}$ or $U_{A'D'B'}$) are compared with those at point F ($U_{A'FB'}$), as shown in Figure 5(e). At each power level, the potential barrier in XOZ plane ($U_{A'FB'}$) is lower than that in lateral plane. That is why the probability of GNP jumping in longitudinal direction is higher than that in lateral. The difference between $U_{A'FB'}$ and $U_{A'C'B'}$ increases with increasing

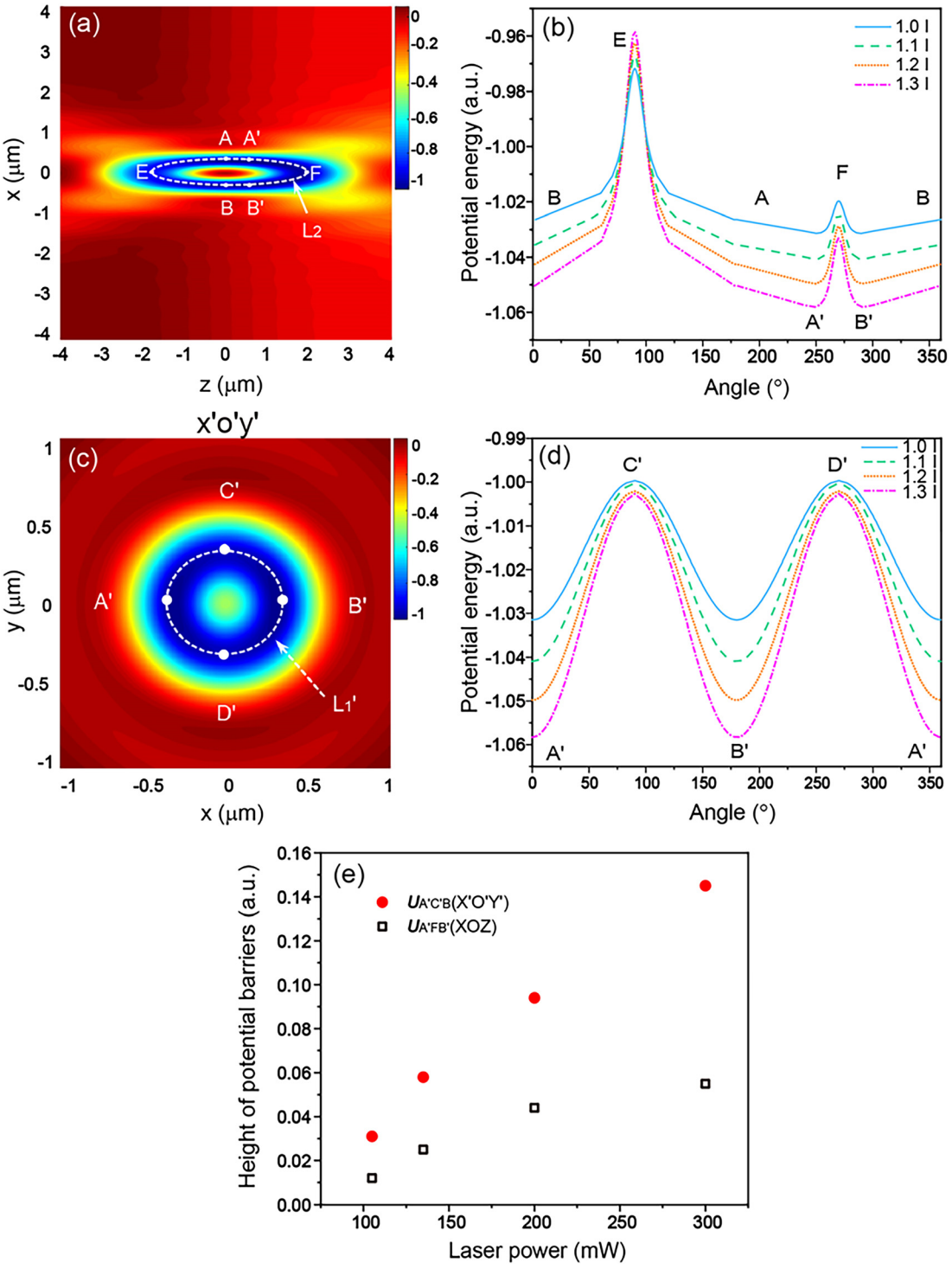

Figure 5: The scattering force plays an important role in the hopping phenomena.
(a) The distribution of potential energy in XOZ plane after considering the scattering force; (b) the potential distribution along L_2 in (a) with different trapping intensity, and the lateral axis indicates the azimuthal angle around focal point in XOZ plane; (c) the distribution of potential energy in the trapping plane after considering scattering force, the dashed circle L_1' indicates the positions of radial minima; (d) the potential distribution along L_1' in (c), and the lateral axis indicates the azimuthal angle around beam center in the X′O′Y′ plane; (e) comparison of the height of potential barriers along L_2 and L_1' under various laser power.

the power, so the probability hopping in XOZ plane become larger and larger, just as we observed in experiments (Figure 4(a)). The scattering force played an important role in the particle hopping phenomena.

A significant feature of TSS is that the small trap separation could be far beyond diffraction limit. Manipulation of colloidal objects with light has been applied in various fields, but the performance is often restricted by the diffraction limit in the traditional optical trapping, especially for the dual (multiple) traps tweezers, as the trapping energy is proportional to light intensity. Some approaches based on plasmonic tweezers provides high manipulating accuracy and efficiency, but suffer from the disadvantage that plasmonic nanostructures are fixed in space, as while as the manipulation scope is limited in near-field. The manipulation based on nonlinear interaction described here provides a distinct full optical method which is capable of breaking diffraction limit, as shown in Figure 4.

The potential well locates in the beam center and split into a spherical shell when laser power is high enough ($aI_0 > 0.5$). The separation distance is determined by the degree of nonlinear polarization (i.e., aI_0) and the NA of objective lens used for trapping, as shown in Figure 6(a), and the simulation is consistent with the experimental results (Figure 4(b)). Figure 2(f) indicates that the separation become larger with increasing the laser power, meanwhile, the depth of potential well ΔU (the potential difference between beam center $\langle U_0 \rangle$ and split position $\langle U_t \rangle$) increases.

When the potential difference is large enough to overcome Brownian motion, the particles can be trapped in the TSS, and that indicates the minimum of separation. In the focal plane, the potential difference is

$$\Delta U = \langle U_0 \rangle - \langle U_t \rangle = -\varepsilon_0 \chi_1 I_0 \cdot \{1 - \exp(-2\rho_t^2) - aI_0[1 - \exp(-4\rho_t^2)]\}. \quad (6)$$

The dependence of trap separation on the potential difference under various NA values are shown in Figure 6(b). The values of potential difference are normalized to minimum of potential shown in Figure 2(f), which is evaluated to be about 50 k_BT. The threshold of potential difference corresponding to diffraction limit is about 20 k_BT, as indicated in Figure 6(b) by the dashed lines. That means even the separation size is beyond diffraction limit, the particles can be effectively trapped. In the case of NA = 0.65, the distance between trap points could be less than 700 nm in our experiment while the diffraction limit is about 790 nm. And in the case of NA = 1.40, the distance between two traps could be less than 100 nm, and this should the smallest separation of

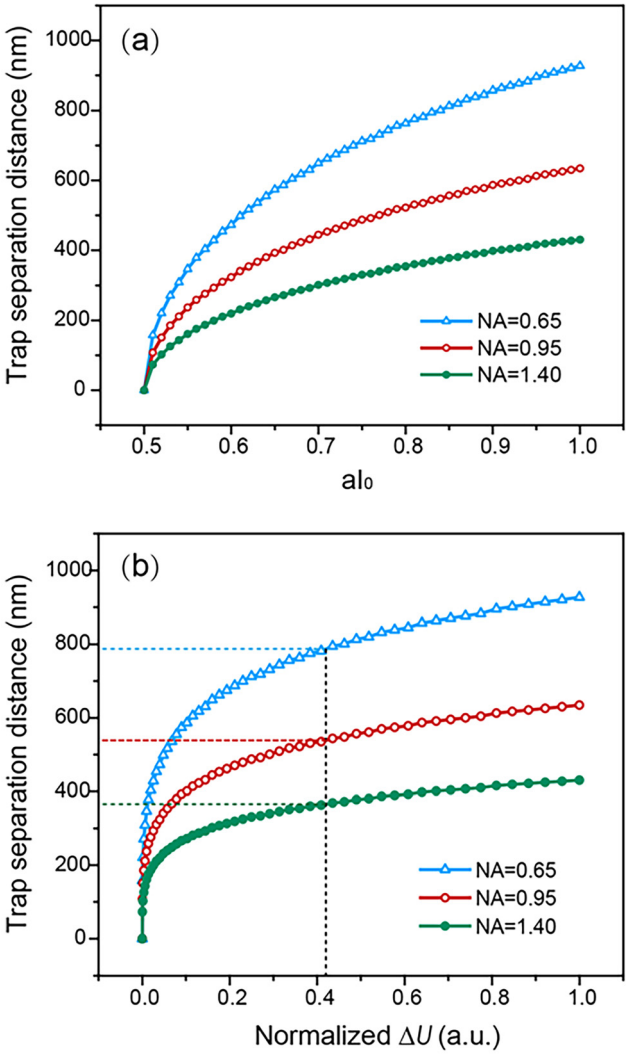

Figure 6: The separation distance is determined by the degree of nonlinear polarization and the numerical aperture of objective lens used for trapping.
(a) The numerical simulation of the trap separation distance on degree of nonlinear polarization, i.e., aI_0 under various NA values; (b) the NA of the dependence of trap separation on the potential difference under various NA values.

multiple traps obtained by the full optical methods without any assisted microstructures-nanostructures, to the best of our knowledge.

In the above experiments, when the trap separations are beyond the diffraction limit, we determined each trap position respectively by using the method of single molecule localization technique by adjusting the concentration of the GNPs to ensure only one particle was trapped. And the positions measured by this method can reflect the actual distance between the two individual potential well. However, when the distance becomes comparable with the particle diameter and particles are simultaneously trapped

in the two split traps, the interaction between the particles should be taken into account. The interaction (typically binding force) between the particles which is caused by the scattering field of the trapped particles [40] is calculated when two 60 nm-diameter particles are trapped simultaneously and the separation is about 100 nm (shown in Figure S6). The results show that the binding force increases when the particles get close to each other, and the binding force between the two particles is larger than the trapping force (about 10^{-1} pN) when the distance becomes comparable with the particle diameter. And with 60 nm-diameter particles, when the splitting separation is down to 100 nm, the two particles cannot be trapped simultaneously. In spite of this, when the radius of the trapped particle decreases, the optical binding force decreases much faster than the gradient force (binding force decreasing with a^6, while gradient decreasing with a^3, see Supplementary material). Figure S6 shows that when the radius decreases to 10 nm, the binding force between the particles decreases to several fN which is much smaller than the corresponding gradient force. So, when trapping with small particles, we can realize dual-trapping beyond diffraction limit with high NA objective and proper trapping power.

5 Conclusion

In conclusion, 3D shell-like potential well can be generated by the nonlinear optical effects when the GNPs were trapped by a linearly polarized fs laser beam in Gaussian mode, and were experimentally demonstrated for the first time. The GNPs can be stably trapped in some special positions, or hop between the trap positions along a route within the 3D shell. And the dynamic hopping of the trapped particle can be controlled by simply adjusting the trapping laser power and polarization, and this might be used as path choice in nanoscale. The more attractive feature of nonlinear optical trapping is, without applying complicated optical systems and on-chip nanostructures, the separation of the subtraps breaks the diffraction limit. Also, the beyond diffraction-limit potential well can be easily controlled by adjusting the trapping power and the material of trapped particles, this may provide opportunities in studies of distance-, material- and orientation-dependent phenomena. This study may be applied in the fields such as microfabrication/nanofabrication, sensing, also can be used for some novel micromanipulations.

Acknowledgments: The authors thank Prof. Hiromi Okamoto from the Institute for Molecular Science (Japan), Prof. Xincheng Yao from Chicago University, Prof. Ya Cheng from East China Normal University and Prof. Lu Li from Shanxi University for their beneficial suggestions and discussions. Y. Jiang acknowledges support from the Strategic Priority Research Program of Chinese Academy of Sciences (Grant no. XDA24020202). This work was partially supported by grants from the National Natural Science Foundation of China (Nos. 11674389, 61675068, 61527824, 11404390).

Author contribution: Y. Jiang initiated and supervised the work. L.H., Y.Q., Y.J. and Y. Jiang designed the experiments, Y.Q., L.H., Y.J. and H.S. carried out the experiments. L.H., Y.Q. and Y. Jiang performed the modelling and simulation. All authors contributed significantly to the discussion of results and the preparation of the manuscript. All the authors have accepted responsibility for the entire content of this submitted manuscript and approved submission.

Research funding: Y. Jiang acknowledges the Strategic Priority Research Program of CAS (Grant no. XDA24020202-1). This work was partially supported by grants from the National Natural Science Foundation of China (Nos. 11674389, 61675068, 61527824, 11404390).

Conflict of interest statement: The authors declare no conflicts of interest regarding this article.

References

[1] Z. Lansky, M. Braun, A. Lüdecke, et al., "Diffusible crosslinkers generate directed forces in microtubule networks," *Cell*, vol. 160, pp. 1159–1168, 2015.

[2] V. Bormuth, V. Varga, J. Howard, and E. Schaffer, "Protein friction limits diffusive and directed movements of kinesin motors on microtubules," *Science*, vol. 325, pp. 870–873, 2009.

[3] M. Rahman, M. Harrington, M. A. Stott, et al., "Optical trapping assisted detection rate enhancement of single molecules on a nanopore optofluidic chip," *Optica*, vol. 6, pp. 1130–1131, 2019.

[4] E. Meyhofer and J. Howard, "The force generated by a single kinesin molecule against an elastic load," *Proc. Natl. Acad. Sci. U. S. A.*, vol. 92, pp. 574–578, 1995.

[5] V. Salakhutdinov, M. Sondermann, L. Carbone, E. Giacobino, A. Bramati, and G. Leuchs, "Optical trapping of nanoparticles by full solid-angle focusing," *Optica*, vol. 3, pp. 1181–1186, 2016.

[6] A. Ashkin, "Optical trapping and manipulation of neutral particles using lasers," *Proc. Natl. Acad. Sci. U. S. A.*, vol. 94, pp. 4853–4860, 1997.

[7] F. W. Sheu, T. K. Lan, Y. C. Lin, S. U. Chen, and C. Ay, "Stable trapping and manually controlled rotation of an asymmetric or birefringent microparticle using dual-mode split-beam optical tweezers," *Opt. Express*, vol. 18, pp. 14724–14729, 2010.

[8] X. C. Yao, Z. L. Li, B. Y. Cheng, X. H. Han, and D. Z. Zhang, "Increasing transverse stability of optical tweezers by using dual-Gaussian beam profile," *Chin. Phys.*, vol. 9, pp. 65–68, 2000.
[9] K. Saito, T. Aoki, T. Aoki, and T. Yanagida, "Movement of single myosin-filaments and myosin step-size on an actin filament suspended in solution by a laser trap," *Biophys. J.*, vol. 66, pp. 769–777, 1994.
[10] M. Capitanio, R. Cicchi, and F. S. Pavone, "Continuous and time-shared multiple optical tweezers for the study of single motor proteins," *Opt. Laser Eng.*, vol. 45, pp. 450–457, 2007.
[11] K. Visscher, S. P. Gross, and S. M. Block, "Construction of multiple-beam optical traps with nanometer-resolution position sensing," *IEEE J. Sel. Top. Quant.*, vol. 2, pp. 1066–1076, 1996.
[12] H. Melville, G. F. Milne, G. C. Spalding, W. Sibbett, K. Dholakia, and D. McGloin, "Optical trapping of three-dimensional structures using dynamic holograms," *Opt. Express*, vol. 11, pp. 3562–3567, 2003.
[13] S. Y. Fu, C. Q. Gao, T. L. Wang, S. K. Zhang, and Y. W. Zhai, "Simultaneous generation of multiple perfect polarization vortices with selective spatial states in various diffraction orders," *Opt. Lett.*, vol. 41, pp. 5454–5457, 2016.
[14] T. Haist and W. Osten, "Holography using pixelated spatial light modulators-part 1: theory and basic considerations," *J. Micro-Nanolith. Mem.*, vol. 14, 2015, https://doi.org/10.1117/1.jmm.14.4.041310.
[15] K. Dholakia and T. Cizmar, "Shaping the future of manipulation," *Nat. Photonics*, vol. 5, pp. 335–342, 2011.
[16] M. Polin, K. Ladavac, S. H. Lee, Y. Roichman, and D. G. Grier, "Optimized holographic optical traps," *Opt. Express*, vol. 13, pp. 5831–5845, 2005.
[17] J. E. Curtis, B. A. Koss, and D. G. Grier, "Dynamic holographic optical tweezers," *Opt. Commun.*, vol. 207, pp. 169–175, 2002.
[18] H. He, N. R. Heckenberg, and H. Rubinszteindunlop, "Optical-particle trapping with higher-order doughnut beams produced using high-efficiency computer-generated holograms," *J. Mod. Opt.*, vol. 42, pp. 217–223, 1995.
[19] Y. Y. Cao, T. T. Zhu, H. Y. Lv, and W. Q. Ding, "Spin-controlled orbital motion in tightly focused high-order Laguerre-Gaussian beams," *Opt. Express*, vol. 24, pp. 3377–3384, 2016.
[20] R. Dasgupta, S. Ahlawat, R. S. Verma, and P. K. Gupta, "Optical orientation and rotation of trapped red blood cells with Laguerre-Gaussian mode," *Opt. Express*, vol. 19, pp. 7680–7688, 2011.
[21] B. H. Jia, X. S. Gan, and M. Gu, "Strong tangential force within a small trapping volume under near-field Laguerre-Gaussian beam illumination," *Opt. Express*, vol. 16, pp. 15191–15197, 2008.
[22] S. Ghosh and A. Ghosh, "All optical dynamic nanomanipulation with active colloidal tweezers," *Nat. Commun.*, vol. 10, 2019, https://doi.org/10.1038/s41467-019-12217-2.
[23] A. N. Grigorenko, N. W. Roberts, M. R. Dickinson, and Y. Zhang, "Nanometric optical tweezers based on nanostructured substrates," *Nat. Photonics*, vol. 2, pp. 365–370, 2008.
[24] M. Righini, A. S. Zelenina, C. Girard, and R. Quidant, "Parallel and selective trapping in a patterned plasmonic landscape," *Nat. Phys.*, vol. 3, pp. 477–480, 2007.
[25] D. Roy, D. Goswami, and A. K. De, "Exploring the physics of efficient optical trapping of dielectric nanoparticles with ultrafast pulsed excitation," *Appl. Optic.*, vol. 54, pp. 7002–7006, 2015.
[26] J. J. J. Nivas, S. He, A. Rubano, et al., "Direct femtosecond laser surface structuring with optical vortex beams generated by a q-plate," *Sci. Rep.*, vol. 5, 2015, https://doi.org/10.1038/srep17929.
[27] Z. S. Huang, Q. F. Dai, S. Lan, and S. L. Tie, "Numerical study of nanoparticle sensors based on the detection of the two-photon-induced luminescence of gold nanorod antennas," *Plasmonics*, vol. 9, pp. 1491–1500, 2014.
[28] K. K. Anoop, A. Rubano, R. Fittipaldi, et al., "Femtosecond laser surface structuring of silicon using optical vortex beams generated by a q-plate," *Appl. Phys. Lett.*, vol. 104, 2014, https://doi.org/10.1063/1.4884116.
[29] S. X. Li and Z. W. Wang, "Generation of optical vortex based on computer-generated holographic gratings by photolithography," *Appl. Phys. Lett.*, vol. 103, 2013, https://doi.org/10.1063/1.4823596.
[30] W. Y. Chiang, A. Usman, and H. Masuhara, "Femtosecond pulse-width dependent trapping and directional ejection dynamics of dielectric nanoparticles," *J. Phys. Chem. C*, vol. 117, pp. 19182–19188, 2013.
[31] Z. Y. Chen, L. M. Hua, and J. X. Pu, "Tight focusing of light beams: effect of polarization, phase, and coherence," *Prog. Opt.*, vol. 57, pp. 219–260, 2012.
[32] Y. Q. Jiang, T. Narushima, and H. Okamoto, "Nonlinear optical effects in trapping nanoparticles with femtosecond pulses," *Nat. Phys.*, vol. 6, pp. 1005–1009, 2010.
[33] L. Gong, B. Gu, G. Rui, Y. Cui, Z. Zhu, and Q. Zhan, "Optical forces of focused femtosecond laser pulses on nonlinear optical Rayleigh particles," *Photon. Res.*, vol. 6, pp. 138–143, 2018.
[34] A. Usman, W. Y. Chiang, and H. Masuhara, "Optical trapping of nanoparticles by ultrashort laser pulses," *Sci. Prog.*, vol. 96, Pt 1, pp. 1–18, 2013.
[35] T. Kudo and H. Ishihara, "Proposed nonlinear resonance laser technique for manipulating nanoparticles," *Phys. Rev. Lett.*, vol. 109, 2012, Art no. 087402.
[36] M. Hoshina, N. Yokoshi, H. Okamoto, and H. Ishihara, "Super-resolution trapping: a nanoparticle manipulation using nonlinear optical response," *ACS Photonics*, vol. 5, no. 2, pp. 318–323, 2018.
[37] T. X. Hoang, X. D. Chen, and C. J. R. Sheppard, "Multipole theory for tight focusing of polarized light, including radially polarized and other special cases," *J. Opt. Soc. Am. A*, vol. 29, pp. 32–43, 2012.
[38] Z. M. Zhang, J. X. Pu, and X. Q. Wang, "Tight focusing of radially and azimuthally polarized vortex beams through a dielectric interface," *Chin. Phys. Lett.*, vol. 25, pp. 1664–1667, 2008.
[39] K. M. Romallosa, J. Bantang, and C. Saloma, "Three-dimensional light distribution near the focus of a tightly focused beam of few-cycle optical pulses," *Phys. Rev. A*, vol. 68, 2003, https://doi.org/10.1103/physreva.68.033812.
[40] K. Dholakia and P. Zemánek, "Colloquium: gripped by light: optical binding," *Rev. Mod. Phys.*, vol. 82, p. 1767, 2010.

Supplementary Material: The online version of this article offers supplementary material (https://doi.org/10.1515/nanoph-2020-0288).